Scaling behavior of the surface roughness of platinum films grown by oblique angle deposition

A. Dolatshahi-Pirouz, M. B. Hovgaard, K. Rechendorff, J. Chevallier, M. Foss, and F. Besenbacher
Interdisciplinary Nanoscience Center (iNANO) and Department of Physics and Astronomy, University of Aarhus, DK-8000 Aarhus C, Denmark

(Received 21 June 2007; revised manuscript received 15 November 2007; published 17 March 2008)

Thin platinum films with well-controlled rough surface morphologies are grown by e-gun evaporation at an oblique angle of incidence between the deposition flux and the substrate normal. Atomic force microscopy is used to determine the root-mean-square value w of the surface roughness on the respective surfaces. From the scaling behavior of w, we find that while the roughness exponent α remains nearly unchanged at about 0.90, the growth exponent β changes from 0.49 ± 0.04 to 0.26 ± 0.01 as the deposition angle approaches grazing incidence. The values of the growth exponent β indicate that the film growth is influenced by both surface diffusion and shadowing effects, while the observed change from 0.49 to 0.26 can be attributed to differences in the relative importance of diffusion and shadowing with the deposition angle.

DOI: 10.1103/PhysRevB.77.115427 PACS number(s): 68.55.−a, 82.45.Mp, 81.15.−z

INTRODUCTION

Recently, there has been an increasing focus on the growth of thin films with rough surface morphologies on the nanometer length scale for applications in areas such as biotechnology, cell and tissue engineering, catalysis, nanoelectronics, optoelectronics, and gas sensing,[1–9] since the surface morphologies and the absolute value of the surface roughness on the nanometer scale may influence the performance of these devices. To be able to successfully synthesize thin films with both a well-defined value of the surface roughness and well-defined surface morphologies, it is of great importance to gain a fundamental understanding of the interplay between the mechanisms involved in the growth process of thin films.

In general, thin film growth is influenced by processes such as surface diffusion and stochastic noise, as well as nonlocal processes such as diffusion-limited aggregation and shadowing effects.[10] Shadowing implies that points of low height receive fewer particles than high points due to the geometrical blocking caused by the larger surface structures. When the deposition is carried out at oblique angles, this effect becomes more pronounced.[11] During growth with shadowing, these competitive growth mechanisms give rise to the formation of columnar structures and lead to a roughening of the surface. Films with well-controlled rough surface morphologies can be grown using the glancing angle deposition (GLAD) technique.[12–19] GLAD is a physical vapor deposition technique in which the flux impinges on a rotating substrate from an oblique angle of incidence (θ), typically $\theta < 20°$, causing an increased shadowing compared to normal incidence.[14,15] The angle of incidence is defined as the angle between the incoming flux and the surface, with $\theta = 90°$ corresponding to the situation where the substrate is normal to the incoming flux. During GLAD, temperature, deposition angle, and the rotation angle can be varied to fabricate well-defined rough morphologies including columnar structures,[12,16,17] zigzag columns,[13–15] and spirals.[18,19]

A standard measure of the surface roughness is the root-mean-square (rms) value w, expressing the variation of the height function $h(r,t)$ over a two-dimensional substrate with linear size L,

$$w(L,t) = \sqrt{\frac{1}{L^2}\sum\left[h(\mathbf{r},t) - \bar{h}(t)\right]^2}, \quad (1)$$

where $\mathbf{r}$ is the position vector, and the mean height is given by

$$\bar{h}(t) = \frac{1}{L^2}\sum h(\mathbf{r},t). \quad (2)$$

A self-affine surface, i.e., a surface where a rescaling, $\mathbf{r} \to b\mathbf{r}$, $h \to b^{\alpha} h$ $(b > 0)$, does not change the statistical properties of the film, exhibits scaling of w,[10,20,21]

$$w(L,t) \sim \begin{cases} t^{\beta} & \text{if } L \gg L_{\text{crossover}} \\ L^{\alpha} & \text{if } L \ll L_{\text{crossover}}, \end{cases} \quad (3)$$

where $L_{\text{crossover}}$ is the crossover length defining the length scale at which $w(L,t)$ reaches saturation,[10] and is roughly related to the spatial correlations ξ along the surface as $L_{\text{crossover}} \approx 4\xi$.[22] The exponents α and β are known as the roughness exponent and the growth exponent, respectively, and together they identify the universality class of a given growth process.[10] If thin films are studied after a given deposition time t, the scaling from Eq. (3) becomes $w(L) \sim w_{\text{sat}} \sim \text{const}$ if $L \gg L_{\text{crossover}}$ and $w(L) \sim L^{\alpha}$ if $L \ll L_{\text{crossover}}$, where w_{sat} is the saturation value of the rms value.

Often, it is important to characterize the rough surfaces in terms of the roughness exponent α and the growth exponent β using the self-affine scaling laws.[10,23–25] From a fundamental point of view, these exponents allow for a classification of the underlying physical phenomena controlling a given growth process. From an applied point of view, a detailed knowledge of the scaling behavior of the surface roughness will make it feasible to synthesize rough surfaces with well-defined roughness and morphological properties. Despite the large interest in using the GLAD technique to generate rough surfaces, the exact relation between the deposition angle θ and the scaling exponents (α, β) is not yet fully understood.

In this study, we demonstrate the ability to synthesize surfaces with well-controlled rough surface morphologies by varying the deposition angle θ and the thickness r of thin

 ©2008 The American Physical Society

TABLE I. The average value of the roughness exponent α for deposition angles θ at different thicknesses r is shown here together with the value of the growth exponent β from the fit in Fig. 3.

	Dep. angle (deg)							
	5		10		35		90	
ρ (ng/cm^2)	r (nm)	α	r (nm)	α	r (nm)	α	r (nm)	α
2.2	35	0.91 ± 0.03			10	0.86 ± 0.07	10	0.92 ± 0.04
4.3	70	0.84 ± 0.05			20	0.86 ± 0.06		
8.2	133	0.87 ± 0.03	84	0.89 ± 0.03	38	0.86 ± 0.06		
13							58	0.92 ± 0.05
15			154	0.81 ± 0.03			70	0.84 ± 0.04
22	396	0.93 ± 0.02	217	0.77 ± 0.06			133	0.80 ± 0.06
32	525	0.87 ± 0.04	315	0.86 ± 0.01				
α_{av}		0.90 ± 0.02		0.86 ± 0.02		0.86 ± 0.04		0.88 ± 0.02
β		0.49 ± 0.04		0.41 ± 0.07		0.28 ± 0.04		0.26 ± 0.01

films. We consider growth conditions without substrate rotation and extend the range of the deposition angles to include the regime $\theta > 20°$ compared to standard GLAD conditions. Moreover, we investigate the scaling behavior of the surface roughness of thin platinum films and find that the roughness exponent α is not influenced by the variations in neither the deposition angle θ nor the film thickness r. In contrast, a correlation is found between the deposition angle θ and the growth exponent β.

EXPERIMENT

The platinum thin films (platinum from Dansk Ædelmetal A/S, DK; 99.9% purity) were grown on gold coated silicon substrates by e-gun evaporation in a vacuum of about 10^{-8} bar with the deposition rate kept constant at 1.5 nm/s, as monitored by a quartz crystal microbalance. The evaporation was performed at room temperature without substrate rotation and with a distance between the evaporation source and the substrate of 25 cm. The deposition was carried out at different oblique deposition angles θ of 90°, 35°, 20°, 12°, 10°, 7°, and 5°. The deposition angle θ was determined with a precision of $<1°$ and defined as 90° when the substrate was perpendicular to the incoming flux. For each deposition angle, the surface mass density (ρ) (representing the total deposited mass per area) was varied from a series of surface mass densities of 2.2×10^{-5}, 4.3×10^{-5}, 8.2×10^{-5}, 13×10^{-5}, 15×10^{-5}, 22×10^{-5}, and 32×10^{-5} g/cm^2 to produce films with different thicknesses since the surface mass density monitored by the quartz crystal microbalance is proportional to the nominal film thickness (given a constant mass density).[26] For the deposition angles θ=5°, 10°, 35°, and 90°, at least three different surface mass densities and corresponding thicknesses were grown to reveal the dependency of the scaling exponents α, β (see Table I) on the deposition angle θ.

As a decrease in the deposition θ angle will reduce the flux of deposited material on a tilted substrate, it was additionally, for a constant choice of surface mass density (8.2×10^{-5} g/cm^2), investigated how different deposition angles θ influence the morphology and resulting film thickness r. For different combinations of surface mass densities and deposition angles, the actual film thickness was measured by a thin film cross-sectional analysis using a Nova NanoSEM 600 (FEI Company) scanning electron microscope (SEM).

The film surface morphology was investigated using atomic force microscopy (AFM), with a commercial Nanoscope IIIa Multimode SPM (Veeco Instruments, Santa Barbara, CA) operated under ambient conditions in the tapping mode at scan frequencies of 1–2 Hz. Conventional silicon cantilevers (NSG01, NT-MDT, Russia) were used with a typical resonance frequency of 150 kHz, a spring constant of 5.5 N/m, an aspect ratio of 3:1, and a tip radius below 10 nm. To investigate if the conventional cantilever applied in this work would lead to misleading results, test was made with two different types of nonconventional cantilevers. A high aspect ratio (10:1) (NSC05, NT-MDT, Russia) cantilever designed to penetrate narrow passages and a high resolution cantilever (NSG10_DLC, NT-MDT, Russia) with a tip radius between 1 and 3 nm which both gave the same results as the conventional one (data not shown). For each film, a series of AFM images of linear dimensions 1, 5.5, and 10 μm was recorded with a resolution of 512×512 pixels at a minimum of three different locations across the surface. The AFM images were subsequently analyzed using a home-written extension to the scanning probe image processor image analysis software package (SPIP)[27] in order to extract the values of the rms roughness w. This analysis program divided each image into subimages, using the size of the subdivision as the length scale L. For each subimage, the rms roughness parameter w was determined, and in this way we could explore the correlation between the rms roughness and length scale L.

RESULTS AND DISCUSSION

In Figs. 1(a)–1(c), cross-sectional SEM images of thin films deposited with a constant surface mass density

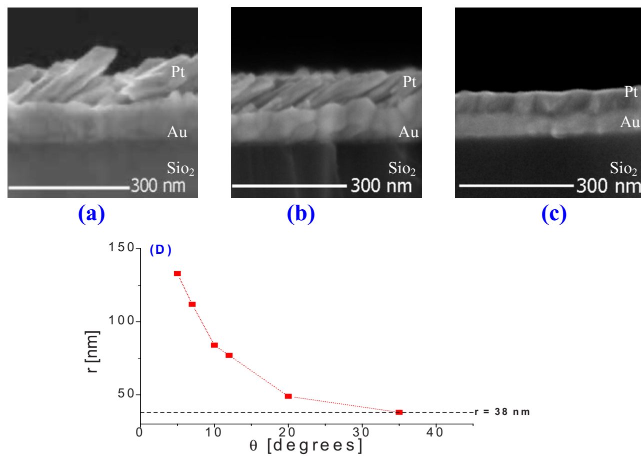

FIG. 1. (Color online) SEM images of platinum films evaporated at different deposition angles θ, with a constant surface mass density of $\rho=8.2\times10^{-5}$ g/cm^2 and nominal thickness of 38 nm. (a) Deposition at $\theta=5°$ results in a thickness $r=133$ nm. (b) Deposition at $\theta=10°$ results in a thickness $r=84$ nm. (c) Deposition at $\theta=35°$ results in a thickness $r=38$ nm. (d) Film thickness r as measured by SEM versus θ.

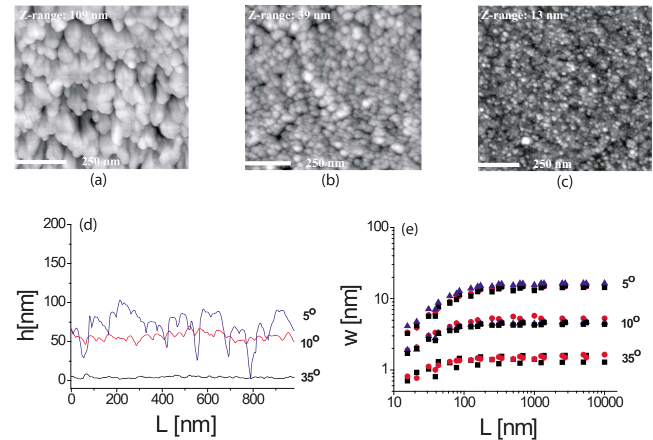

FIG. 2. (Color online) [(a)–(c)] AFM images of the surface morphology of thin platinum films deposited at different deposition angles θ and a constant surface mass density $\rho=8.2\times10^{-5}$ g/cm^2. (a) Deposition at $\theta=5°$ results in a thickness 133 nm. (b) Deposition at $\theta=10°$ results in a thickness 84 nm. (c) Deposition at $\theta=35°$ results in a thickness 38 nm. The columnar structures slowly begin to dominate the surface morphology as the deposition angle is decreased. (d) The respective line scans from the images are shown, illustrating how the surface becomes rougher as the deposition angle is decreased. (e) The rms roughness w as a function of the length scale L for the respective AFM images [(a)–(c)]. For each measurement on a specific location on the surface (represented by a square, circle, or a triangle), the root-mean-square roughness follows a power law until the crossover length is reached and then saturates.

$\rho=8.2\times10^{-5}$ g/cm^2 and deposition angles θ ranging from 35° to 5° are shown. To investigate the correlation between the nominal thickness [the nominal thickness is defined as the thickness determined by the quartz crystal microbalance (QCM) measurements using a platinum mass density of 21.47 g/cm^2 (bulk density)] as measured by quartz crystal microbalance and the actual thickness of the films when the deposition angle θ is varied, a cross-sectional analysis of the SEM images was performed. The variation of the actual (as measured by SEM) film thickness r as a function of deposition angle θ is displayed in Fig. 1(d). For $\theta=35°$, the actual film thickness is identical to the nominal thickness (the desired thickness), but for smaller angles θ, the measured film thickness increases as the deposition angle decreases. From a closer examination of the SEM images in Fig. 1, it is further noticed that thin films evaporated with the same surface mass density at high incidence angles ($\theta=35°$) have higher effective mass densities than those evaporated at low incidence angles ($\theta=5°$, 10°), and in the latter case, large interior voids appear to develop. In general, the variation of the actual film thickness with the substrate tilt angle is caused by two competing mechanisms that both depend on the deposition angle. (i) For a certain deposition time, the incoming flux decreases as the deposition angle is lowered, leading to a decrease in the film thickness for depositions at an oblique angle compared to normal incidence. (ii) Conversely, the thickness of the thin film increases with the deposition angle due to an increased film porosity for depositions at a low angle of incidence compared to normal incidence. In the current study, the lower flux capture for the glancing angle depositions is compensated by changing the deposition time in order to keep the deposited surface mass density constant. The observed variation of thin film thickness r with changes in deposition angle θ [Fig. 1(d)] is therefore attributed exclusively to the different porosities of the films. Therefore, we have to rely on the film thicknesses measured from the SEM images to elucidate the influence of the deposition angle on the scaling exponents α, β for film deposition at angles $\theta<35°$.

To investigate the rough surface morphologies at different deposition angles θ and how the scaling behavior of the surface roughness depends on the deposition angle, we turn to the AFM images depicted in Figs. 2(a)–2(c). A clear difference in the surface morphologies is observed between the images taken at different deposition angles θ. From Fig. 2(a), we further observe that a preferred growth direction is present, corresponding well to the anisotropic columnar growth observed by SEM. A similar preferential growth direction in a deposition experiment without substrate rotation was observed by Mayr and Samwer[28]. Moreover from the linescans, shown in Fig. 2(d) it is evident, that a decrease in θ leads to larger and more pronounced columnar structures, resulting in rougher films at smaller deposition angles. The self-affinity of the films was investigated by using a well-established method in the literature,[10,23–25,29] where the rms surface roughness of the thin films w is plotted against the length scale L [Fig. 2(e)]. From Fig. 2(e), it is observed that w increases and saturates at a certain length scale [$L_{crossover}$, cf. Eq. (3)]. As the deposition angle decreases, $L_{crossover}$ becomes larger. Since the $L_{crossover}$ value and the correlation length are roughly related ($L_{crossover}\approx4\xi$), this means that the mound size should increase according to Ref. 30. Turning to the AFM images in Figs. 2(a)–2(c) again, it is clearly seen that the mound structures become broader as the deposition angle is lowered from 35° to 5° in accordance to the observations made in Fig. 2(e).

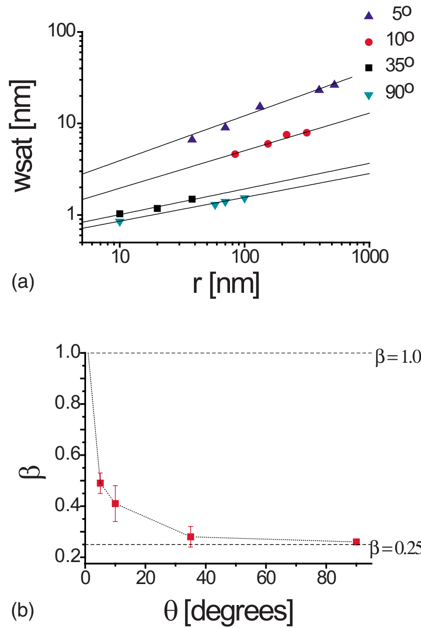

FIG. 3. (Color online) (a) w_{sat} versus film thickness r is shown in a log-log plot. Data are fitted by a power law $w_{sat}(r)=ar^{\beta}$. (b) β plotted versus θ. A graph is drawn relying on the fitted β value from (a) (red squares) and a criteria where $\beta=1.0$ and $\beta=0.25$ as the deposition angles go toward its limits $\theta=0°$ and $\theta=90°$.

The roughness exponent α is found by fitting the data points in the small length regime ($L \ll L_{crossover}$) with a power law, while the saturation value of the rms roughness w_{sat} is found by fitting the data in the large length scale regime ($L \gg L_{crossover}$) with a constant.

Table I summarizes the results on the roughness exponent α for different film thicknesses r and at different deposition angles θ. We observe that within the experimental uncertainty, the roughness exponent α remains close to 0.90, independent of the deposition angle θ and film thickness r. This value is similar to the ones observed by AFM in other experiments where deposition with GLAD technique was used.[29–31] In Ref. 29, $\alpha \cong 1$ was found for chromium deposition at a deposition angle of 1°, and in Ref. 31, it was shown that for thin tantalum films, α changed from 0.75 to 0.93 as the deposition angle θ was varied between 5° and 40°.To investigate whether a correlation exists between the growth exponent β and the deposition angle θ, we plot w_{sat} against r and determine the growth exponent β for each deposition angle θ by fitting the data with a power law, as shown in Fig. 3(a). The power law is in accordance to the relation between the thickness r and growth exponent β, as indicated in Eq. (3), when taking the proportionality between r and time t into consideration [cf. Eq. (3)]. We notice that β decreases from 0.49 ± 0.04 to 0.26 ± 0.01 in a nonlinear fashion as θ increases from 5° to 90° [Fig. 3(b)], showing a clear deposition angle dependence.

Values of the growth exponent β for films grown by oblique angle incidence have, to our knowledge only , been reported for a deposition angle at 1°,[29] where $\beta=1$ was found. According to theoretical considerations, the value of β is larger than 0.5 when the shadowing mechanism dominates the growth process and with diffusion still playing an active role and close to 1 when no surface diffusion is present.[32] Without shadowing, simulations performed in $d=2+1$ dimensions, incorporating surface diffusion and random deposition,[33,34] show that the growth exponent value is $\beta=0.25$, close to what we have observed for deposition at normal incidence $\theta=90°$, where shadowing is not expected to have a large impact on the deposition process. Our values of β for deposition angles in the grazing angle regime are in accordance to these findings within the experimental uncertainties. In general, surface diffusion is an activated process, which depends on the substrate temperature and substrate chemistry.[10] It is therefore most plausible that the growth process transition observed from our results occurs due to an enhanced shadowing effect as the deposition angle is lowered, with the surface diffusion remaining constant. The variations of the growth exponent value as the deposition angle θ is changed ($0.26 \pm 0.01 < \beta < 0.49 \pm 0.04$) suggest a transition from a growth regime controlled mainly by surface diffusion to a regime with a more pronounced contribution from the shadowing effect. This observation is in accordance with what we have observed from the SEM images [Figs. 1(a)–1(c)] and AFM images [Figs. 2(a)–2(c)], where the rough surface morphology becomes smoother as the deposition angle θ is increased and the columnar structures less pronounced. Similar competitive effects during thin film growth have been reported before.[30,35]

Concerning the roughness exponent α since it is retrieved at small length scales where local growth processes are present rather than nonlocal processes, it is not expected to be dependent on the deposition angle θ. Interestingly, the obtained value for the roughness exponent α is very close to the one reported for a surface diffusion dominated film growth.[33,34] The growth exponent β is retrieved from the roughness data at large length scales, where the surface roughness is influenced by nonlocal processes. It is therefore not surprising that β depends on the deposition angle.

CONCLUSION

Platinum thin films were grown by oblique angle deposition and their surface morphologies and roughness were subsequently investigated by SEM and AFM. From the SEM images, we found that the film thickness r decreases for an increasing deposition angle θ, while keeping the deposited surface mass density ρ constant. This observation leads to the conclusion that the films become more porous as the deposition angle approaches grazing incidence. Furthermore, it was found that the roughness exponent α did not depend on the deposition angle θ unlike the behavior of the growth exponent β. The variation of the growth exponent as a function of deposition angle θ indicates a transition from a surface diffusion dominated growth process to a growth process controlled by geometrical shadowing effects. These results are of significant interests both from a fundamental perspective elucidating the growth mechanism behind oblique angle deposition experiments and from a practical perspective opening new possibilities for designing and growing nanostructured surfaces with a well-defined roughness and morphology at the nanoscale.

ACKNOWLEDGMENTS

We gratefully acknowledge the financial support from the Danish Research Councils to the Centre for NeuroEngineering (CNE) and Interdisciplinary Nanoscience Center (iNANO) and from the European Commission to the FP6 STREP project: NANOCUES. We would also like to thank Folmer Lyckegaard for the production of the thin films used in this work.

[1] D. Barreca, A. Gasparotto, C. Maccato, C. Maragno, and E. Tondello, Langmuir **22**, 8639 (2006).
[2] A. Vantomme, Z.-Y Yuan, G. Du, and B.-L. Su, Langmuir **21**, 1132 (2005).
[3] L. A. Bauer, N. S. Birebbaun, and G. J. Meyer, J. Mater. Chem. **14**, 517 (2004).
[4] A. Dolatshahi-Pirouz, M. B. Hovgaard, K. Rechendorff, M. Foss, J. Chevallier, and F. Besenbacher (unpublished).
[5] P. Roach, D. Farrar, and C. C. Perry, J. Am. Chem. Soc. **127**, 8168 (2005).
[6] K. Rechendorff, M. B. Hovgaard, M. Foss, V. P. Zhdanov, and F. Besenbacher, Langmuir **22**, 10885 (2006).
[7] M. J. Dalby, S. J. Yarwood, M. O. Riehle, H. J. H. Johnstone, S. Affrossman, and A. S. G. Curtis, Exp. Cell Res. **276**, 1 (2002).
[8] B. Wojciak Stothard, A. Curtis, W. Monaghan, K. MacDonald, and C. Wilkinson, Exp. Cell Res. **223**, 426 (1996).
[9] N. Gadegaard, E. Martines, M. O. Riehle, K. Seunarine, and C. D. W. Wilkinson, Microelectron. Eng. **83**, 1577 (2006).
[10] A. L. Barabasi and H. E. Stanley, *Fractal Concepts in Surface Growth* (Cambridge University Press, Cambridge, 1995).
[11] R. P. U. Karunasiri, R. Bruinsma, and J. Rudnick, Phys. Rev. Lett. **62**, 788 (1989).
[12] C. Buzea, G. Beydaghyan, C. Elliot, and K. Robbie, Nanotechnology **16**, 1986 (2005).
[13] K. Robbie, M. J. Brett, and A. Lakhtakia, Nature (London) **384**, 616 (1996).
[14] K. Robbie, G. Beydaghyan, T. Brown, C. Dean, J. Adams, and C. Buzea, Rev. Sci. Instrum. **75**, 1089 (2004).
[15] K. Robbie and M. J. Brett, J. Vac. Sci. Technol. A **15**, 1460 (1997).
[16] C. M. Zhou and D. Gall, Appl. Phys. Lett. **88**, 203117 (2006).
[17] C. M. Zhou and D. Gall, Thin Solid Films **515**, 1223 (2006).
[18] R. Messier and V. V. Venugopal, J. Vac. Sci. Technol. A **18**, 1538 (2000).
[19] S. Kennedy, M. J. Brett, O. Toader, and S. John, Nano Lett. **2**, 59 (2002).
[20] T. Halpin-Healy and Y.-C. Zhang, Phys. Rep. **254**, 215 (1995).
[21] J. Krug, Adv. Phys. **46**, 139 (1997).
[22] G. Palasantzas, Phys. Rev. B **48**, 14472 (1993).
[23] H. Iwasaki and T. Yoshinobu, Phys. Rev. B **48**, 8282 (1993).
[24] T. Yoshinobu, A. Iwamoto, and H. Iwasaki, Jpn. J. Appl. Phys., Part 2 **33**, L67 (1994).
[25] A. Iwamoto, T. Yoshinobu, and H. Iwasaki, Phys. Rev. Lett. **72**, 4025 (1994).
[26] G. Sauerbrey, Z. Phys. **155**, 206 (1959).
[27] Image Metrolgy A/S, 2800 Kgs. Lyngby, Denmark, see www.imagemet.com for more information.
[28] S. G. Mayr and K. Samwer, J. Appl. Phys. **91**, 2779 (2002).
[29] D. Le Bellac, G. A. Niklasson, and C. G. Granqvist, Europhys. Lett. **32**, 155 (1995).
[30] M. Pelliccione, T. Karabacak, C. Gaire, G.-C. Wang, and T.-M. Lu, Phys. Rev. B **74**, 125420 (2006).
[31] K. Rechendorff, M. B. Hovgaard, J. Chevallier, M. Foss, and F. Besenbacher, Appl. Phys. Lett. **87**, 073105 (2005).
[32] J. T. Drotar, Y.-P. Zhao, T.-M. Lu, and G.-C. Wang, Phys. Rev. B **62**, 2118 (2000).
[33] S. Das Sarma and P. Tamborenea, Phys. Rev. Lett. **66**, 325 (1991).
[34] D. Wolf and J. Villanin, Europhys. Lett. **13**, 389 (1990).
[35] T. Karabacak, J. P. Singh, Y.-P. Zhao, G.-C. Wang, and T.-M. Lu, Phys. Rev. B **68**, 125408 (2003).